J Mater Sci (2010) 45:929–935
DOI 10.1007/s10853-009-4022-6

Electromigration-enhanced intermetallic growth and phase evolution in Cu/Sn–58Bi/Cu solder joints

Hongwen He · Guangchen Xu · Fu Guo

Received: 8 August 2009 / Accepted: 5 November 2009 / Published online: 17 November 2009
© Springer Science+Business Media, LLC 2009

Abstract This paper presents some experimental observations relative to the influence of elevated current densities on the intermetallic growth and phase evolution in Cu/Sn–58Bi/Cu solder joints. Three samples were stressed with different current densities of 10^4, 1.2×10^4, and 1.4×10^4 A/cm^2, respectively, for 80 h. The abnormal polarity effect of electromigration (EM) on chemical reactions at the cathode and the anode was investigated as well as the effect of EM on phase segregation in the two-phase eutectic microstructure. Results indicate that electric current enhances the growth of IMC layer at the cathode and retards it at the anode due to the Bi accumulation acting as a barrier layer with current density of 10^4 A/cm^2. However, when current density increases, the electrical force dissolves the IMC at the cathode into the solder. More and more intermetallic precipitates formed due to the dissolution of Cu into the solder at the cathode side with increased current densities, leading to a very different morphology at the anode and the cathode interfaces, one being planar and the other being very irregular. It can be concluded that the chemical force and the electrical force are the main driving forces contributing to the IMC growth at both interfaces.

Introduction

As device miniaturization demands smaller and smaller interconnects, the current density goes up, as does the probability of circuit failure induced by electromigration (EM). This is a very important subject which has demanded and attracted much attention. EM is one of the most important reliability issues in solder joint. Commonly, it is considered as the movement of metal atoms in the direction of electron flow resulting from the momentum transfer between conducting electrons and diffusing metal atoms [1–3]. EM failure has been investigated extensively in order to understand and control this phenomenon in metallization. There has been a limited number of works regarding the effect of EM on IMC growth in the solder/Cu system. Polarity effect of IMC growth at the interfaces was first reported by Chen's group in 1998 [4]. Tu and co-workers investigated EM behaviors of Cu/Sn–37Pb/Cu, Cu/Sn–3.5Ag/Cu and Cu/Sn–3.8Ag–0.7Cu/Cu reaction couples, which proved that there was a polarity effect on IMC growth and the growth rate at the anode had a parabolic dependence on time [5–7].

In the present study, EM behavior in the Cu/Sn–58Bi/Cu end-to-end structural solder joints was studied with high current densities of 10^4, 1.2×10^4, and 1.4×10^4 A/cm^2 at room temperature. Sn–58Bi solder has already been considered as one of the most promising lead-free solders applied in electronic packaging. It is widely used for the connection of heat-sensitive components because of its low melting point. Chen et al. has reported the Bi accumulation phenomenon at the anode side due to EM which seriously degrades the solder joint reliability because of the brittleness behavior of the Bi layer formation [8–10]. The present study focused on the fundamental EM effects on the IMC growth and phase evolution in the solder joints.

H. He (✉) · G. Xu · F. Guo
College of Materials Science and Engineering, Beijing University of Technology, 100 Ping Le Yuan, Chaoyang District, 100124 Beijing, People's Republic of China
e-mail: hhw@emails.bjut.edu.cn

Experimental

The preparation procedure of the Cu/Sn–58Bi/Cu solder joint includes five steps: alloy smelting, solder balls

production, soldering, inlaying, and polishing. So first of all, pure Sn and Bi metal particles with purity of 99.9 wt% were used as raw materials. Sn and Bi metal particles were weighed accurately according to the mix percentage and then put into an Al_2O_3 ceramic crucible, and meanwhile eutectic salt (KCl + LiCl) with weight ratio of 1.3:1 was used to cover the surface of the particles to prevent oxidation during smelting. The crucibles were placed in an induction furnace at 550 °C for about 20 min. The molten alloy was then held on for about 40 min and mechanically stirred every 10 min with a glass rod to promote uniformity of the solder alloy [11, 12]. The molten solder was finally chill cast into a rod ingot in a mold. Solder balls were made of solder alloy with uniform droplet spraying equipment in our laboratory. Solder balls were placed between two copper wires with 500 μm in diameter and placed on a hot plate fixed in the soldering platform designed and built by ourselves. The specific soldering procedure was described in detail in our previous study [13–15]. Figure 1 shows the OM picture of the as-reflowed Cu/Sn–58Bi/Cu solder joint. Unlike the line-to-bump geometry of a flip chip solder joint, the end-to-end structure has a very uniform current density distribution throughout the solder joint due to the special one-dimensional configuration. The current crowding happens at the electron entry and exit region can be eliminated effectively. However, the Joule heating induced by high current stressing will still affect the EM reliability. Therefore, the heat dissipation plate was installed on the solder joint and together mounted with epoxy resin to dissipate the Joule heating. The heat dissipation plate was made of aluminum. Figure 2 shows the schematic drawing of the Cu/Sn–58Bi/Cu solder joint after inlaying with heat dissipation plate. Grinding machine was applied to reduce the dimension of the samples, followed by grid sandpapers, and finely polished with Al_2O_3 suspension. Microstructural and compositional analysis was examined by an S-3400N

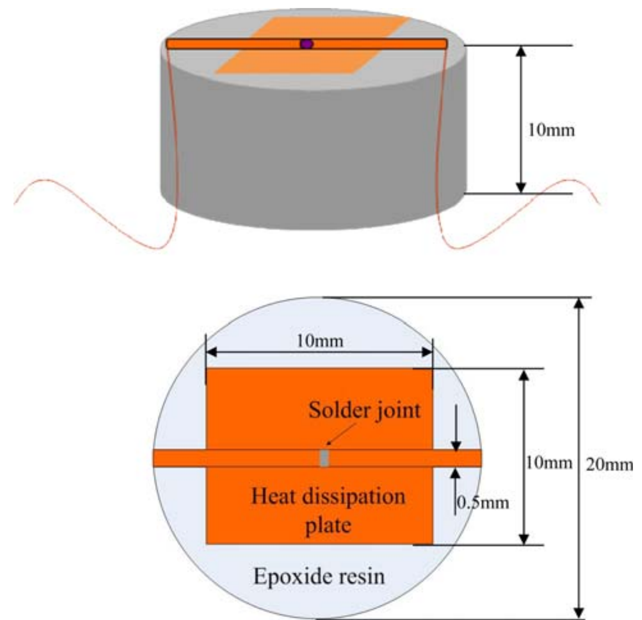

Fig. 2 Schematic drawing of the solder joint after inlaying

scanning electron microscope (SEM) equipped with an energy dispersive X-ray spectroscopy (EDX) system.

The samples were connected with a DC power supply to provide a constant current flow. A thermocouple was attached on the surface of the solder joint to detect the temperature fluctuation. The measured temperature tended to be stable at 80–100 °C when applying different current stressing. For convenient observation, a Microview MVC 2000 Camera was mounted on the optical microscope equipped with relevant software to monitor and record the EM process. Figure 3 shows the schematic drawing of the EM test. The average current density is calculated by dividing the current value by the virtual cross-sectional area which the electrons pass.

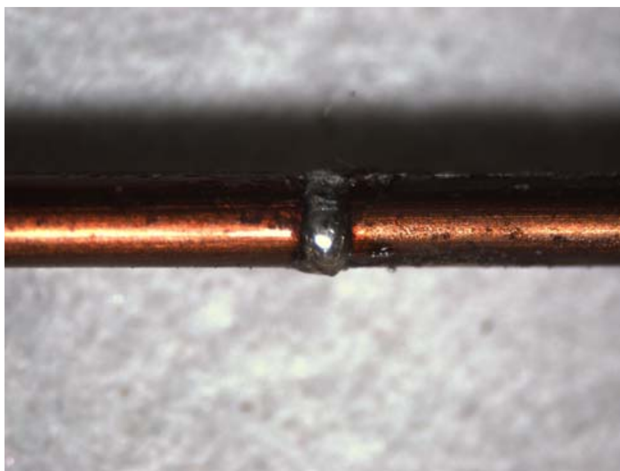

Fig. 1 OM picture of the as-reflowed Cu/Sn–58Bi/Cu solder joint

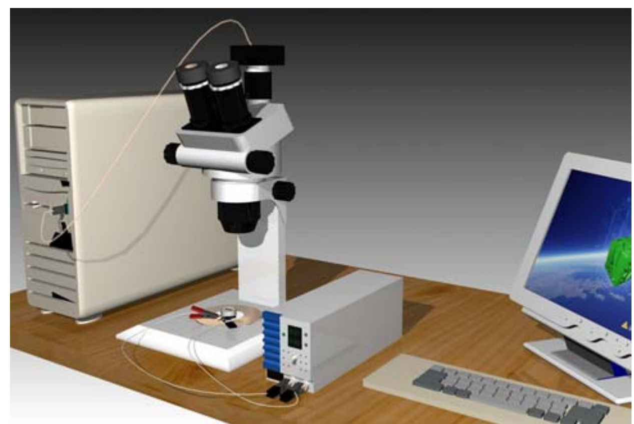

Fig. 3 Schematic drawing of the electromigration test

Results and discussion

Figure 4 shows a typical uniform two-phase microstructure of Sn–58Bi before current stressing, the bright white Bi-rich phase and the dark gray Sn-rich phase, where Fig. 4a and b represents the low and high magnified SEM images, respectively. The formation of two thin intermetallic compound (IMC) layers with average thickness of 1.0 μm at the two solder interfaces can be seen. EDX compositional results revealed that the IMC layers were Cu_6Sn_5. The thickness of the IMC layer is determined by dividing the area of IMC by the length of interface. The measurements of area and length are obtained from digital SEM pictures and imaging processing software. The direction of the current flow was from the anode to the cathode but the direction of the electrons was on the contrary as can be seen in Fig. 4a.

Microstructural evolution with different current densities

Figure 5 shows the microstructure of the Sn–58Bi solder joint with current density of 10^4 A/cm^2 after current

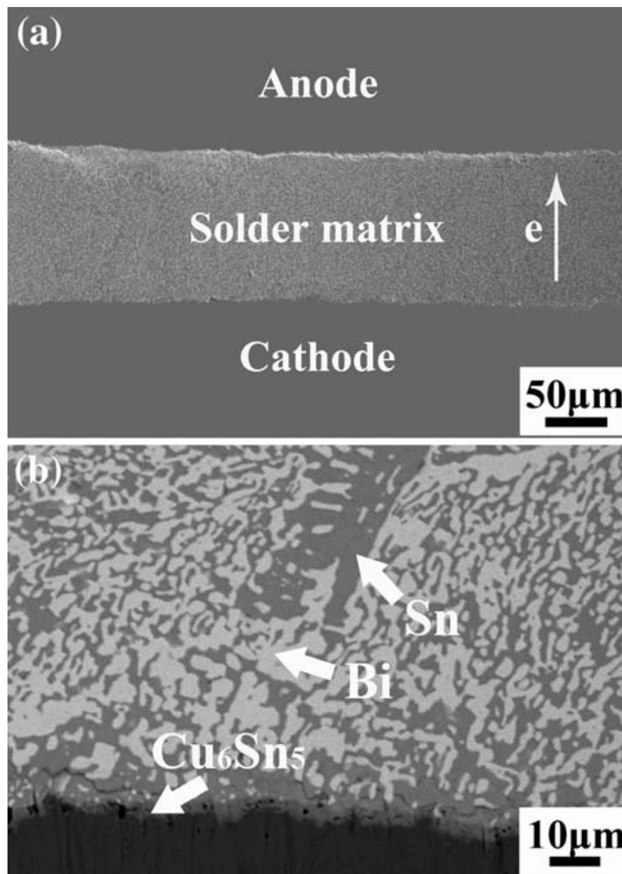

Fig. 4 Low (**a**) and high (**b**) magnified SEM morphologies of the Sn–58Bi solder matrix before current stressing

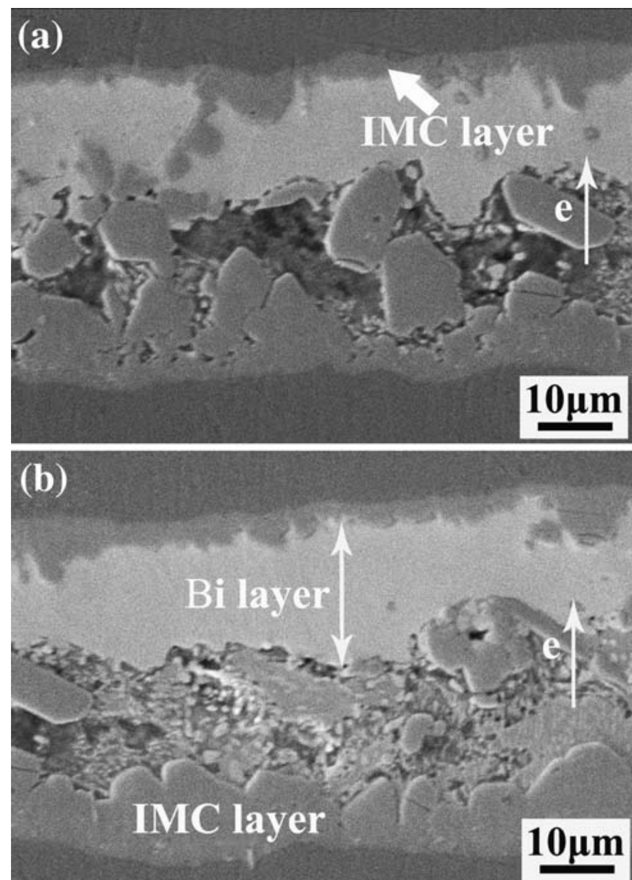

Fig. 5 Microstructural morphologies of the Sn–58Bi solder joint with current density of 10^4 A/cm^2 for 80 h

stressing for 80 h, where Fig. 5a and b represents different regions of the solder matrix. Compared to the microstructure prior to current stressing, there were obvious changes occurred in the solder matrix. First of all, the uniform two-phase microstructure could not be observed any more. The IMC layers at both the anode and the cathode thickened for a prolonged period of time. The thickness of the IMC layer at the anode increased to 3.7 μm, however, the thickness of the IMC at the cathode increased to 10.4 μm. Furthermore, the IMC morphology was different. A layer-type IMC layer formed at the anode interface and scallop-type IMC layer formed at the cathode interface. It was interesting to find that a Bi layer with thickness of about 13.2 μm formed between the IMC layer and the solder matrix at the anode. It should be noted that some IMC at the cathode had spalled into the solder. In other words, the IMC had detached from the Cu substrate and moved into the solder as shown in Fig. 5a.

Figure 6 shows the microstructure of the Sn–58Bi solder joint with current density of 1.2×10^4 A/cm^2 after current stressing for 80 h, where Fig. 6a–d represents the full image, the anode, the cathode, and OM image at the anode, respectively. Compared with the microstructure in Fig. 5,

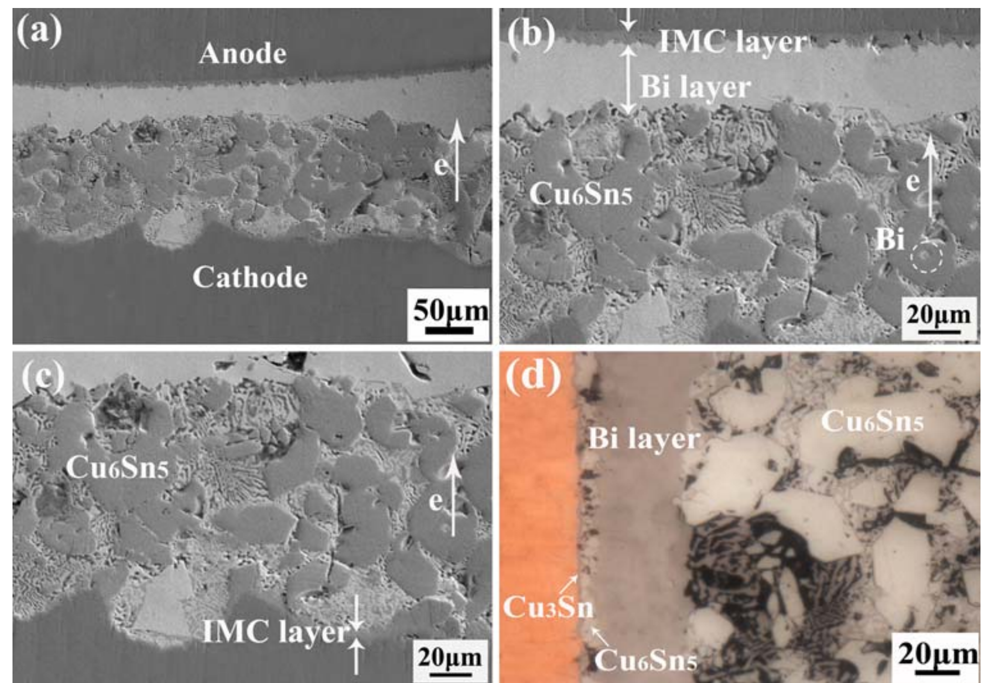

Fig. 6 Microstructural morphologies of the Sn–58Bi solder joint with current density of 1.2×10^4 A/cm^2 for 80 h: **a** full image, **b** at the anode, **c** at the cathode, **d** OM image at the anode

serious phase evolution occurred in the solder matrix. The thickness of the layer-type IMC layer at the anode increased to 5.6 μm. Composition of the IMC layer was Cu_3Sn and Cu_6Sn_5 with thickness of 1.8 and 3.8 μm, respectively. Because of the contrast difference observed with optical microscope, different color of the Cu_3Sn and Cu_6Sn_5 layer can be seen in Fig. 6d. Meanwhile, the Bi layer accumulated at the anode interface grew much thicker than the case with current density of 10^4 A/cm^2. It increased to about 42.6 μm as can be clearly seen in Fig. 6a and b. The thick Bi layer formation sufficiently suggests that significant mass transport has occurred due to EM effect. Bi atoms migrated from the cathode to the anode which in accordance with the electron direction. It should be noted that the Cu substrate at the cathode was not straight again but undulating. This in turn suggested that Cu dissolution and migration toward the anode occurred and was not entirely uniform during the current stressing which correspondingly resulted in the different morphology. The average solder thickness became 169.8 μm, which was 16.2 μm larger than that before current stressing. This indicated that 10.6 μm-thick Cu at the cathode dissolved into the solder matrix if the IMC growth at the anode interface was taken into consideration.

What was the most remarkable in Fig. 6 was that a number of intermetallic precipitates with different sizes formed in the solder matrix. EDX results revealed that these intermetallic precipitates were Cu_6Sn_5. In addition, some eutectic SnBi microstructure remained among these Cu_6Sn_5 precipitates. It was worth noticing that some Bi phases appeared in the Cu_6Sn_5 precipitates as if they were embedded there as shown in Figs. 6b and 7c. The question how these Bi phases had been incorporated into the precipitates needs to be addressed. It was not likely that Bi would have marked solubility in IMC or migrated into the IMC. Therefore, it was more probable that Bi had been frozen into the IMC during the formation of the IMC. Furthermore, a few voids and cracks formed both at the anode interface and the cathode interface.

Figure 7 exhibits the microstructure of the Sn–58Bi solder joint with current density of 1.4×10^4 A/cm^2 after current stressing for 80 h, where Fig. 7a–c represents the full image, the anode and the cathode, respectively. The microstructural evolution induced by EM was similar with that of in Fig. 6. Bi segregation at the anode and the Cu_6Sn_5 precipitates formation in the solder matrix also happened. However, the Bi accumulation and the Cu_6Sn_5 precipitates were commingled together rather than separated as indicated in Fig. 6. Moreover, some eutectic SnBi structure remained at the cathode interface rather than among the Cu_6Sn_5 precipitate. The thickness of the IMC layer at the anode interface became 6.8 μm. The Cu substrate at the cathode was also undulating with thickness of about 4.6 μm. The average solder thickness increased to 129.6 μm which was 21.8 μm larger than that before current stressing. This indicated that about 15 μm-thick Cu at the cathode dissolved into the solder matrix. Voids and cracks also formed at the anode and the cathode interfaces. This would be owing to the stress generation induced by current stressing and Joule heating. Additionally, different diffusion coefficient of elements can also promote the void formation at the interfaces.

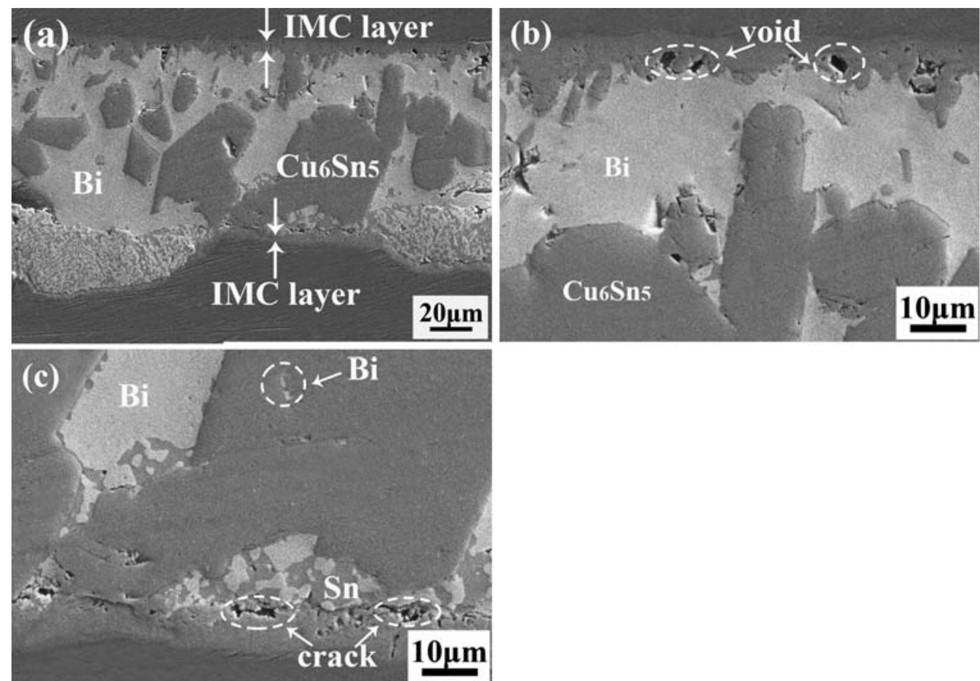

Fig. 7 Microstructural morphologies of the Sn–58Bi solder joint with current density of 1.4×10^4 A/cm^2 for 80 h: **a** full image, **b** at the anode, **c** at the cathode

IMC growth and phase evolution kinetics

Based on the three Sn–58Bi solder joints stressed with different current densities of 10^4, 1.2×10^4, and 1.4×10^4 A/cm^2 for 80 h given above we can conclude that the IMC growth at the two interfaces are enhanced by the elevated current densities. What is significant in the above observation is that many Cu_6Sn_5 precipitates formed in the solder matrix and the Bi layer formed at the anode, which indicates that Bi and Cu are transported from the cathode to the anode. Due to the dissolution of IMC into the solder at the cathode, a very different morphology formed at the anode and the cathode interfaces, one being planar and the other being very irregular. Figure 8 and Table 1 illustrate the IMC layer and Bi layer thickness at the cathode and the anode interfaces with different current densities.

As atoms are forced to depart from the equilibrium positions, it is expected to cause compressive stress in the direction of the electron flow and produce tensile stress in an upstream direction with respect to the electron flow [16, 17]. With the current stressing time increasing, the Bi phases act as the main diffusing species at the initial duration. When they reach the anode, compressive stress forms due to the superfluous atomic flux. Therefore, the stress gradient is come into being near the anode region. In order to relieve the stress gradient, the Sn atoms are driven out of the anode on the contrary direction. Consequently, the Bi layer formation is produced at the anode interface due to the departure of Sn atoms. As Sn atoms reach the cathode interface, they will react with Cu and enhance the IMC growth. Hence, the Cu–Sn reaction at the cathode is

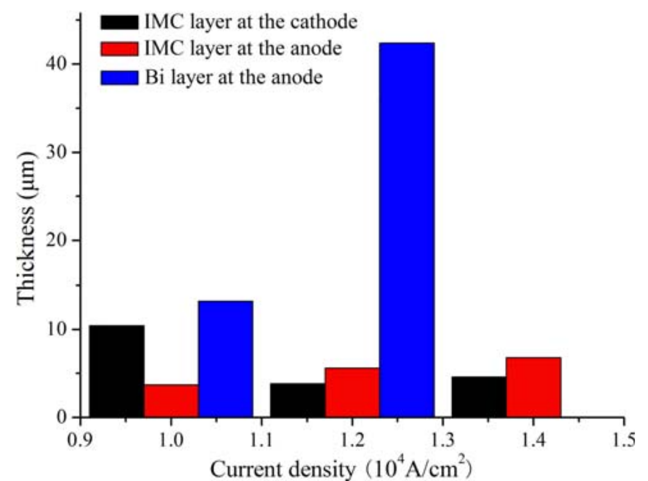

Fig. 8 IMC layer and Bi layer thickness at the cathode and the anode interfaces with different current densities

enhanced by the continuing arrival of Sn. Nevertheless, because of the Bi layer formation at the anode, it is as a function of a barrier layer to block the migration of Cu atoms to the anode. This can well interprets the different IMC thickness at the two interfaces that the thickness of the IMC layer at the cathode is much larger than that at the anode with current density of 10^4 A/cm^2.

It is generally accepted that EM is the result of a combination of thermal and electrical effects on mass transport [18]. The electric current enhances the diffusion of Cu in IMC since Cu is the dominant diffusing species in IMC growth. The Cu diffusion is in the same direction as the electron current, and therefore enhances the growth of

Table 1 IMC layer and Bi layer thickness in Cu/Sn–58Bi/Cu solder joint with different current densities for 80 h

Current density (10^4 A/cm^2)	IMC thickness at the cathode (μm)	IMC thickness at the anode (μm)	Bi layer thickness at the anode (μm)
1.0	10.4	3.7	13.2
1.2	3.8	5.6	42.4
1.4	4.6	6.8	–

Cu_3Sn and Cu_6Sn_5. However, the electric current may enhance the dissolution of IMC into the solder. As can be seen in Figs. 6 and 7, many Cu_6Sn_5 precipitates formed in the solder matrix with elevated current densities. These Cu_6Sn_5 precipitates may form in two ways: one is the Cu atoms are driven to the anode and react with Sn atoms to form Cu_6Sn_5 precipitates in the solder matrix. Another one is the IMC layer at the cathode interface has spalled into the solder induced by EM. According to the Joule law $Q = I^2Rt$, because I is a fixed value provided by DC power supply, therefore Q is correlative with R and t. Consequently, much more Joule heating is produced after a long time current stressing resulting in the increase of the temperature. Owing to the high atomic diffusivity and migration in high temperature, Cu atoms and IMC at the cathode dissolve into the solder and react with the Sn atoms to form a number of Cu_6Sn_5 precipitates in the solder matrix.

On account of the reasons explained above, it is expected that the Cu_6Sn_5 precipitates formation and migration mechanism is controlled by the Cu dissolution at the cathode to the solder enhanced by current stressing through the solder matrix. Therefore, considering the combined Joule heating effect and EM effect, both the IMC growth and the Bi segregation is both thermally activated and electrical accelerated.

As we have discussed, there are two driving forces contributing to the change of thickness of the IMC. They are the chemical force and the electrical force. The flux equation for the mass transportation can be given as [5, 6]

$$J = J_{\text{chem}} + J_{\text{em}} = C\frac{D}{kT}\left(-\frac{\partial \mu}{\partial x}\right) + C\frac{D}{kT}Z * ej\rho$$

where C is concentration, D is diffusivity, kT has the usual meaning, $\partial\mu/\partial x$ is chemical potential gradient, Z^* is effective charge number, e is electron charge, ρ is resistivity, and j is current density.

At the cathode side, the chemical force enhances the IMC, whereas, the electrical force dissolves the IMC. These two forces compete during the entire EM process. The solid-state aging study has illustrated that the layer-type IMC growth driven by chemical potential gradient force alone is diffusion-controlled. The growth rate satisfies $\mathrm{d}x/\mathrm{d}t \propto A/x$. This means that when a layer thickness approaches zero, the growth velocity $\mathrm{d}x/\mathrm{d}t$ goes to infinity. Thus, the layer cannot disappear in the diffusion-controlled mode. In other words, the chemical potential gradient becomes infinite as the layer thickness approaches zero. When the electrical force is weak, the chemical force may exceed the electrical force, and the growth of IMC can occur at the cathode interface [5, 6]. Therefore, the growth of IMC at the cathode was enhanced as the current density was 10^4 A/cm^2 as can be seen in Fig. 5. When the electrical force is comparable to the chemical force or exceeds it, the IMC will spall into the solder as can be seen in Figs. 6 and 7. However, in my opinion, EM is a time-dependent process. If the current stressing time continues to increase when the current density is 10^4 A/cm^2, the IMC layer at the cathode will also dissolve into the solder.

Conclusion

Effects of different current densities of 10^4, 1.2×10^4, and 1.4×10^4 A/cm^2 for 80 h on Cu/Sn–58Bi/Cu solder joints at room temperature were investigated. The IMC growth at the two interfaces was enhanced by the EM. Many Cu_6Sn_5 precipitates formed in the solder matrix and the Bi layer formed at the anode, which indicated that Bi and Cu were transported from the cathode to the anode. Due to the dissolution of IMC into the solder at the cathode, a very different morphology formed at the anode and the cathode interfaces, one being planar and the other being very irregular. Concerning the microstructural evolution in the solder matrix, there is no doubt that the chemical force and the electrical force are the main driving forces contributing to the IMC growth and dissolution at the anode and the cathode interfaces with elevated current densities.

Acknowledgements The authors acknowledge the financial support of this work from the New Century Talent Support Program, Ministry of Education, and the Funding Project PHR (IHLB).

References

1. Nah JW, Paik KW, Suh JO, Tu KN (2003) J Appl Phys 94:7560
2. Gan H, Tu KN (2005) J Appl Phys 97:063514-1
3. Lin YH, Hu YC, Tsai CM, Kao CR, Tu KN (2005) Acta Mater 53:2029
4. Chen S-W, Chen C-M, Liu W-C (1998) J Electron Mater 27(11):1193
5. Huynh QT, Liu CY, Chen C, Tu KN (2001) J Appl Phys 89(8):4332
6. Ou S, Tu KN (2005) In: Proceedings of the 55th ECTC, vol 2, pp 1407–1415
7. Liu CY, Chen C, Liao CN, Tu KN (1999) Appl Phys Lett 75(1):58
8. Chen C-M, Huang C-C (2007) J Alloy Compd 461:235
9. Chen C-M, Huang C-C (2008) J Mater Res 23(4):1051

10. Chen C-M, Huang C-C, Liao C-N et al (2007) J Electron Mater 36(7):760
11. Chen ZG (2002) J Electron Mater 31(10):1122
12. Chen ZG (2003). PhD Thesis, Beijing University of Technology
13. Xu GC, He HW, Guo F (2009) J Electron Mater 38:273
14. He HW, Xu GC, Hao H, Guo F (2007) ICEPT. Shanghai, China, p 225
15. Guo F, Xu GC, He HW (2009) J Mater Sci 44(20):5595. doi:10.1007/s10853-009-3787-y
16. Ma HT (2009) J Mater Sci 44(14):3841. doi:10.1007/s10853-009-3521-9
17. Cheng F, Nishikawa H, Takemoto T (2008) J Mater Sci 43(10):3643. doi:10.1007/s10853-008-2580-7
18. Chao BH-L, Zhang X, Chae S-H, Ho PS (2009) Microelectron Reliab 49:253